applied sciences

MDPI

Article

Turbocharger Axial Turbines for High Transient Response, Part 1: A Preliminary Design Methodology

Glen Walsh, Marco Berchiolli, Gregory Guarda and Apostolos Pesyridis *

Department of Mechanical and Aerospace Engineering, Brunel University, London UB8 3PH, UK; 1313519@brunel.ac.uk (G.W.); 1436706@brunel.ac.uk (M.B.); 1307125@brunel.ac.uk (G.G.)

* Correspondence: a.pesyridis@brunel.ac.uk; Tel.: +44-1895-267901

Received: 14 January 2019; Accepted: 20 February 2019; Published: 26 February 2019

Abstract: This paper proposes a preliminary design algorithm for application of a turbocharger axial turbine, based on turbine thermodynamic analysis and the Ainley-Mathieson performance model that converges to the optimal design based on a set of input parameters and engine boundary conditions. A design space sweep was conducted, and a preliminary design was generated with a predicted total to static efficiency of 74.94%. CFD (computational fluid dynamics) was used to successfully validate the algorithm and show the preliminary design had a total to static efficiency of 73.98%. The design also produces the required power to support steady-state operation of the compressor in both free flow conditions and with a constrained pressure outlet.

Keywords: turbocharging; axial turbines; preliminary design

1. Introduction

The cost of fuel in the UK over the last fifteen years is presented in Figure 1. The price of fuel increases faster than inflation, suggesting it will be a greater factor in the consumers' thought process on purely economic grounds. Because of this, automotive manufacturers are implementing and researching methods to improve the fuel economy of their vehicles. One way to do this is by reducing the size of engines in the fleet, known as downsizing. Smaller engines are intrinsically more fuel efficient, demonstrated experimentally by Fraser et al. [1], also leading to an overall reduction in CO_2 emissions.

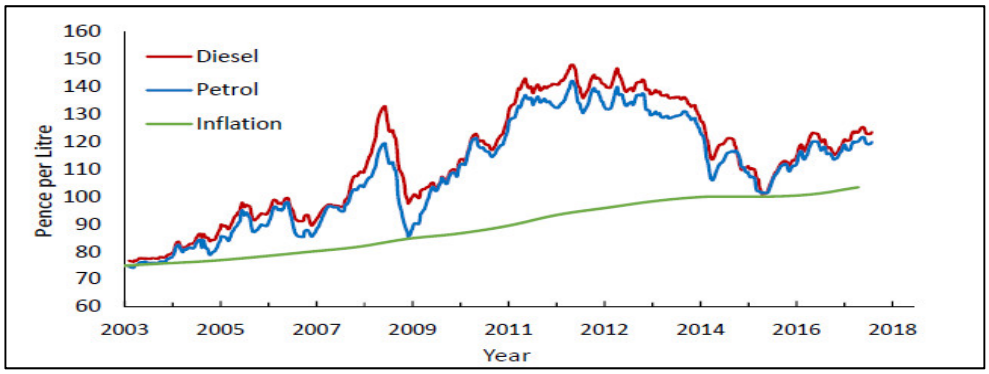

Figure 1. UK fuel prices at pump and UK inflation rates normalised to fuel prices (consumer price indexing), data from Department for Business, Energy & Industrial Strategy (2018) and Rate Inflation (2018) [2,3].

Downsizing the engine in a vehicle will reduce its power output and performance, therefore additional boosting technologies that can increase the power density of an engine are vital in sustaining

the downsizing trend; turbochargers are one such boost device. A study by Simmons and Giakoumis [4] suggests turbochargers accounted for 33% of net fuel savings from all technologies among new vehicles sold over two representative years in the United States. This is a multi-faceted benefit, as it incentivises turbocharged vehicles as a financially responsible option, as well as playing to the social pressures towards more environmentally friendly transport.

Turbo-lag is the primary target for improvement by current day turbocharger manufacturers. It has become such a focus in the industry because of the poor reputation it has with drivers, making them feel less connected to the vehicle and reducing the quality of the driving experience, particularly in high performance turbocharged vehicles. 'Boost on demand' is a concept that resonates with the manufacturers of high-performance vehicles, needing immediate and predictable responses to the drivers control inputs [5].

While improving the turbine power output is one method to tackle turbo lag, the other is to decrease the rotational moment of inertia of the turbochargers rotating assembly. The inertia of the system represents the amount of torque needed to produce a level of angular acceleration around the rotational axis. By decreasing this quantity an equivalent power generation will spool the turbocharger up faster, providing increased boost to the engine, faster. Focusing on the turbine as a route to better inertia, replacing the conventional, bulky radial turbine with an advanced, lightweight axial device has potential to improve the transient response of the boost system and the whole vehicle, while not sacrificing steady-state performance. This defines the problem with current turbocharging technology and highlights the necessity for research on the axial turbine in the automotive environment.

Despite the dominance of radial devices in small automotive turbine applications, there is clear evidence to indicate the benefits the axial turbine can offer. The specific speed and specific diameter is a useful way of normalising a turbine for a direct performance comparison with devices of completely different scales. Dixon and Hall [6] suggest that radial turbines significantly drop off in efficiency above specific speeds of 0.8. Pesyridis et al. [7] show that for the modelled operating conditions of a Ford eco-boost 1.6 litre petrol engine, lead to a turbine specific speed and specific diameter that support the implementation of an axial device.

In addition to potential performance benefits, the rotational moment of inertia of the axial turbine is intrinsically lower than a radial equivalent. Early testing by Rahnke [8] demonstrated that the turbocharger equipped with an axial turbine reached full boost pressure 25–40% faster than the radial equivalent. This potential for improvement in transient performance was a significant motivating factor for the current research programme.

In more recent years, Honeywell have demonstrated the DualBoost system, which uses a lower radius axial turbine to further improve the transient performance by 25% and more effectively combat turbo-lag. This design also features a two-sided, low diameter compressor wheel for a further improved transient profile [9]. This illustrates how the automotive industry is actively trying to tackle the requirement for 'boost on demand', even at the cost of device efficiency.

Despite obvious advantages axial turbines are predominantly found in aerospace and large power generation applications. A key challenge is the corresponding decrease in efficiency with a decrease in size. For power ranges of a few kilowatts such as in automotive turbocharging, blade heights for axial turbines are very small with a disproportionate resultant increase in the effect of leakage paths which have to minimized with finer manufacturing tolerancing, making the employment of axial turbocharger turbine a costly proposition. Hence, increases in aerodynamic efficiency are of paramount importance in the successful employment of such designs.

2. Axial Turbine Loss Modelling

The accuracy of the preliminary design process is wholly reliant on the loss predictions used to calculate stage thermodynamics and flow velocity vectors. Wei [10] has compiled the most prominent loss models for axial turbines and identified the components of the total system pressure loss.

The Soderberg correlation [11] provides the simplest three-dimensional function for blade performance. It uses the flow turning angle, basic blade geometry and the Reynolds number to predict pressure losses over a blade. The functions are based on a large amount of experimental cascade data and was considered too simplistic for the level of preliminary design aimed for.

The second option considered was the model suggested by Craig and Cox [12]. They lay out a comprehensive prediction model based on summing the profile loss, secondary loss, annulus loss and tip leakage loss. Despite its accuracy, the Craig & Cox model was not considered suitable for this design process, as the intention was to fully automate the performance prediction. Due to the high number of calculations reliant on cascade data it would be very difficult and time consuming to implement the full model in an automated algorithm, as the system would have to 'read' all the graphs automatically.

Ainley and Mathieson [13] builds a total blade loss co-efficient from the same elements as the Craig & Cox method and assumes pressure loss coefficients are not influenced by the flow Mach number, therefore avoiding shock losses. This means the accuracy of the model is compromised under highly supersonic conditions. Due to the conventional flow speeds and temperatures in a turbocharger, velocities significantly above the transonic range are not expected so does not preclude the use of this model. As the blade geometries anticipated from the turbocharger axial turbine involve aspect ratios near to 1, the Dunham & Came prediction allows for increased accuracy over the conventional Ainley-Mathieson model [10]. This applies a correlation for the prediction of the secondary flow loss coefficient, as opposed to basing it on cascade data as a function of annulus geometric properties.

It also introduces a new function for evaluating the tip clearance loss. Yaras and Sjolander [14] compare the most popular loss models based on their tip-leakage predictions and show that the Dunham & Came correction results in tip loss components significantly larger than the other available methods. Their review is general to all turbines, so the guidance of Dixon [6] and Saravanamuttoo et al. [15] was followed for this low aspect ratio application. The 3D loss model employed for the system was the Ainley-Mathieson prediction with Dunham & Came correction.

Wei [10] found that the Craig & Cox and Ainley-Mathieson models demonstrated the same performance trends compared with experimental data, so the decision to use the simpler method should not penalise the accuracy of the obtained results. The chosen performance prediction method requires five cascade readings, from three different graphs. This was considered acceptable complexity for the automated preliminary design process.

3. MATLAB Turbine Design System

Based on systems of equations from literature, a MATLAB algorithm was developed that can perform the preliminary design process of a single stage axial turbine based on a given set of boundary conditions and design parameters. As the thermodynamic calculations involved in velocity triangle derivation are based on assumed values of blade row loss components and stage efficiency, it was necessary to iterate the solution to converge to a realistic design. The operational process of the algorithm is presented in Figure 2. Initial attempts to iterate the loss components were based on the two-dimensional meanline losses from purely thermodynamic equations. These proved to be highly unstable and would diverge with most combinations of input parameters. The solution was to allow the system to finish a full design procedure for each iteration up to and including the geometry calculations. This way, instead of the meanline losses, the efficiency and loss components would be fed back from the Ainley-Mathieson performance calculations. It was a concern that this would significantly increase the computational time required to generate the design space meta-data as each iteration would contain a full run of the system as opposed to just the meanline analysis, however this method proved to be very stable, and was always able to converge within 10 iterations. This meant that it was more accurate, more stable and more computationally efficient.

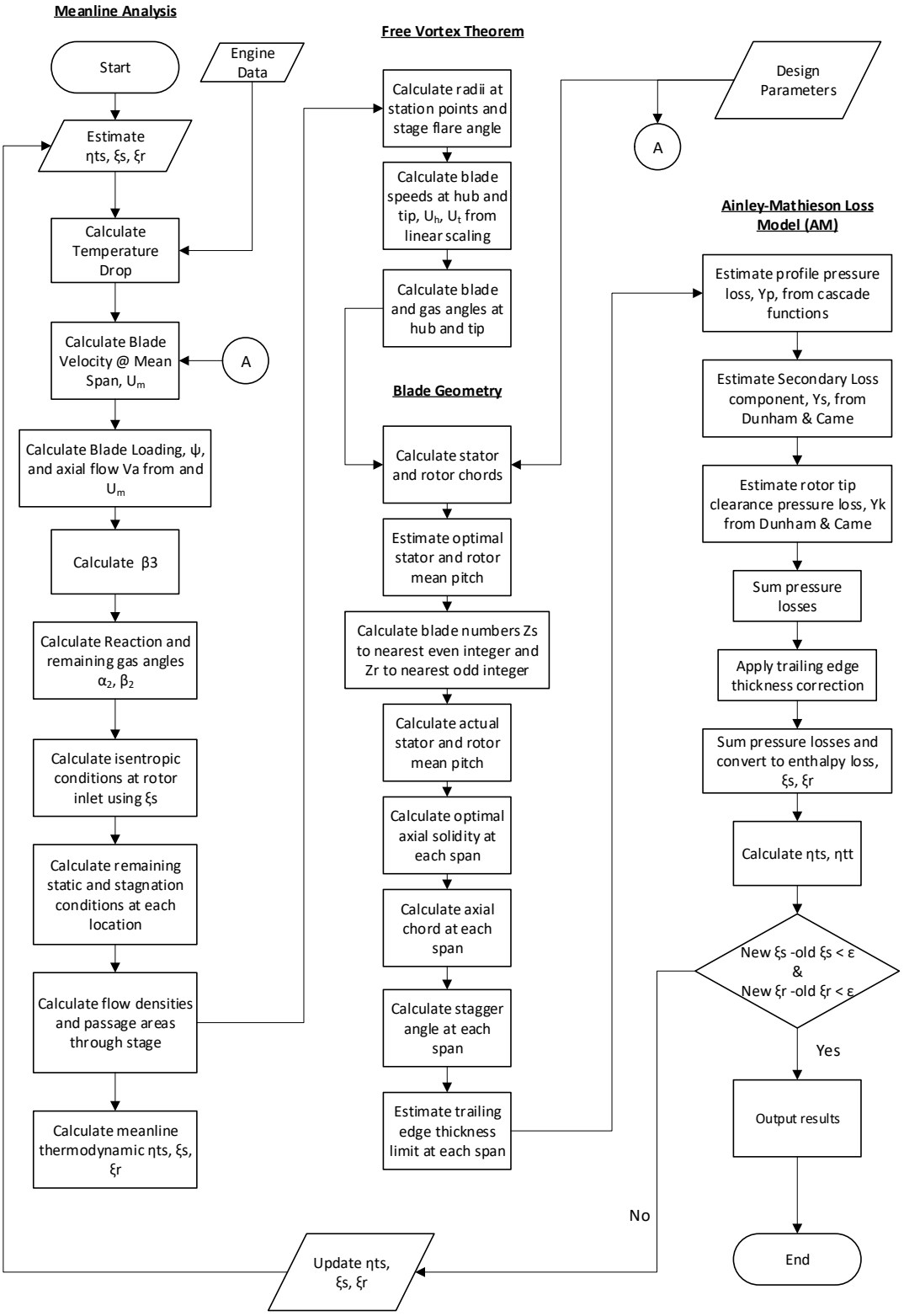

Figure 2. Flowchart of MATLAB turbine design algorithm procedure.

The boundary conditions specified in Table 1 are obtained directly from an internally created Ricardo WAVE engine model of the Ford eco-boost 1.6 litre petrol engine operating with the scaled GT1548 turbocharger performance maps and constitute the design operating point of the engine. The design parameter D_{max} specifies the maximum diameter of the turbine, which will occur at the tip

trailing edge of the rotor blade. It is then decided whether the axial turbine should be sized equal to the radial turbine, which should lead to improved efficiency [6] or whether a smaller turbine will meet the engine requirements while providing improved transient performance due to lower rotational moment of inertia.

Table 1. Boundary conditions and design parameters required for meanline analysis.

Boundary Conditions	Design Parameters
T_{t1}, P_{t1}, P_3, N, $\dot{m}$, γ, C_p	D_{max}, ϕ, α_3, HTR

The hub to tip ratio design parameter, HTR, is enforced at the rotor exit. In combination with the known tip radius from D_{max} this will allow the mean radius to be determined. The flow coefficient, ϕ, and the rotor absolute gas exit angle, α_3, are harder to visualise, so are an important part of the brute force style design space sweep discussed in next section. The first stage of the turbine design procedure is the meanline analysis, utilising the equations presented by the Equations (A1) to (A15). An estimate for the isentropic total to static efficiency is provided in Equation (A4) as a first guess for the convergence process. For this article a starting value equal to the radial turbine performance at design conditions was chosen. This way an improvement in efficiency should be seen through the iterations, although it is proven from algorithm validation section that this value does not influence the final result, but merely increases the number of iterations required to converge.

These equations have determined the relationship between the components of the fluid velocity and the rotation of the rotor blades. The calculated angles are used to set blade inlet and outlet angles that correspond to the flow at the design point and increase the blade row efficiency under these conditions [16]. It is usually assumed that the absolute velocities are equal in magnitude at the stator inlet and rotor exit for convenience, such that $V_1 = V_3$ [6,17]. However, as the value of V_3 will be important later in the calculation of the total to static efficiency it was decided to determine it more accurately using Equation (A13).

Following this, the system thermodynamics are established via the Equations (A16) to (A27). The fluid properties are assessed via the isentropic relationships at each station point, which are used to establish the passage areas throughout the stage. Like the earlier estimation made for total to static efficiency, this procedure requires an initial estimate for the stator enthalpy loss coefficient, ξ_{stator}. Again, this assumption is proven to not impact the final results. An estimate of $\xi_{stator} = 0.06$ was chosen, based on examples from Peng and Saravanamuttoo et al. [15,17].

The meanline thermodynamic losses are then calculated using Equations (A28) to (A32) and are to be compared with the Ainley-Mathieson predictions once a design has been selected. The rotor enthalpy losses are directly evaluated from the difference between stator enthalpy loss estimate and the predicted stage enthalpy loss from the total to static efficiency for the current iteration. The stator meanline loss component is recalculated by considering the pressure loss over the stator and converting it to an enthalpy loss via the isentropic Mach number relationship in Equation (A30).

Free vortex equations (Equations (A33) to (A39)) are applied to calculate the variation in fluid velocity angles at hub (0% span) and tip (100% span), along with the tangential blade speed at each span for the leading and trailing edge. Due to the flow velocities the fluid must be considered as compressible, so the passage area is expanding through the stage, leading to a variation in linear velocity between the leading and trailing edge of the rotor blade. Consequently, velocity triangles for rotor inlet and exit cannot be plotted with a shared U vector at the hub and tip.

At this point additional design parameters are required to generate the three-dimensional blade geometry. These parameters are described in Table 2. While it is possible to combine each of these parameters as a generic value for both the stator and rotor, it was decided to introduce additional design flexibility and broaden the design space by separating them.

The Zweifel coefficient describes the tangential aerodynamic force generated by the blade as a function of blade surface area and can be used to estimate an optimal value of the axial solidity, σ.

The axial solidity relates the size of the blade with the spacing between blades such as to minimise unnecessary frictional losses from a large chord length while managing the additional flow separation losses incurred from a shorter, more strongly curved blade [16].

Table 2. Design parameters for blade geometry creation.

Zweifel Coefficient	$C_{L,stator}$, $C_{L,rotor}$
Aspect Ratio	AR_{stator}, AR_{rotor}
Optimum Pitch/Chord Ratio	$(s/c)_{opt,\ stator}$, $(s/c)_{opt,\ stator}$

Using the previously determined turbine information and these design parameters the blade geometry is generated meridionally and in the aerofoil profile plane from Equations (A40) to (A55).

To reduce the rotor vibrational response and ensure the blade rows are balanced to avoid natural frequencies best practice is to use an odd number of rotor blades and an even number of stator blades [15,16]. To enforce this, the values of Z_{rotor} and Z_{stator} are rounded to the nearest odd and even integer respectively. The pitch is then recalculated exactly, by rearranging the blade number calculations for pitch and using the new integer blade count.

With the blade geometry fully modelled, the final stage of the iteration loop is to evaluate the turbine stage performance according to the Ainley-Mathieson estimation with a modification for the Secondary loss components and correlation for rotor tip clearance from Dunham & Came. The calculation of profile losses is subject to a correction factor based on the maximum thickness/chord ratio of the aerofoil profile at mid span, however this value is not obtainable at this point within MATLAB. The correction factor is 1 at a maximum thickness/chord of 0.2. Preliminary investigation into the aerofoil profiles produced by this design algorithm resulted in values between 0.15 and 0.2, so it was deemed acceptable to ignore this correction.

Five values in the performance calculations for the Ainley-Mathieson method are directly obtained from cascade data presented in graphs. As the MATLAB algorithm is iterating based on the performance parameters it needs to be able to 'read' these graphs automatically. To do this, an online graphics digitiser was used to probe sample points on the function lines from Ainley and Mathieson [13], which have been used to construct best fit fourth order polynomials. The MATLAB algorithm chooses function lines either side of the blade outlet angle being analysed and then linearly interpolates between them to accurately predict profile loss.

The plots of these functions can be seen in Figure 3, Figure 4 along with the original cascade data for comparison. Figure 5 shows the best fit fourth order polynomial for the trailing edge thickness correction. This is used to directly calculate the correction factor based on the trailing edge thickness determined in the geometry calculations. The value of $Y_{P,stator}$ is obtained directly from Figure 3. $Y_{P,rotor}$ is calculated with a combination of Figures 3 and 4 and Equation (A56).

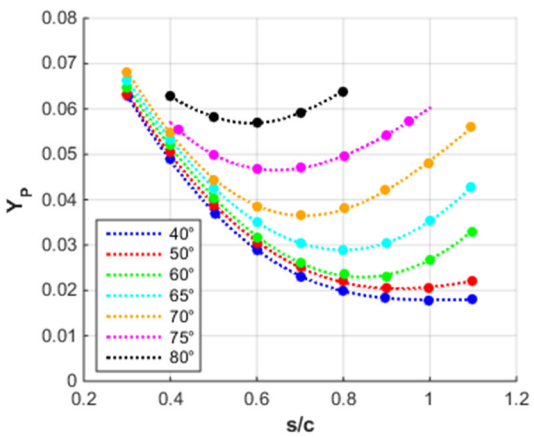

Figure 3. Cascade plots for profile loss where inlet angle = 0°.

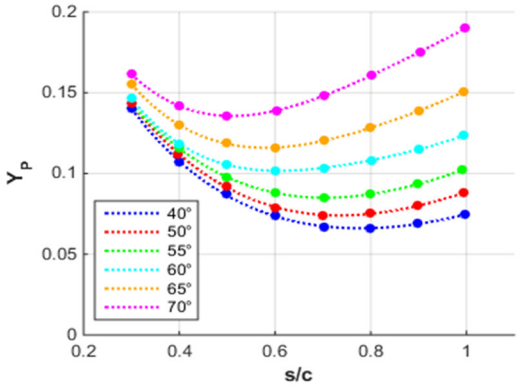

Figure 4. Cascade plots for profile loss where inlet angle = outlet angle.

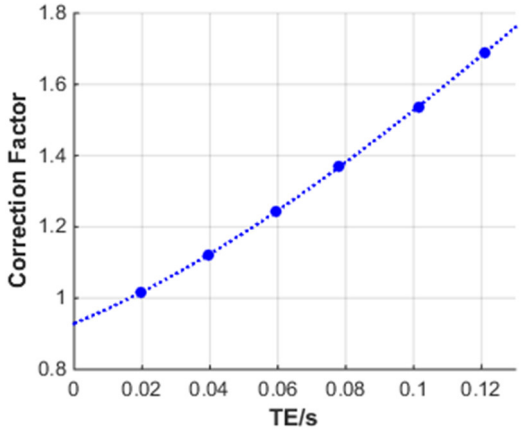

Figure 5. Cascade plot for trailing edge thickness loss correction factor.

Where the blade angles being analysed are outside of the ranges covered by the cascade data the profile losses are set as ten, which immediately reduced the efficiency to near zero and identifies the design as poor. This was necessary to prevent MATLAB errors while sweeping the design space.

As per Figure 2, the Ainley-Mathieson prediction for total to static efficiency and enthalpy losses are fed back into the meanline analysis until both convergence criteria have been met. The convergence criteria is defined below in Equations (1) and (2), where $\varepsilon = 10^{-9}$.

$$\frac{\left|\zeta_{stator,\,new} - \zeta_{stator,\,old}\right|}{\zeta_{stator,\,old}} < \varepsilon \tag{1}$$

$$\frac{\left|\zeta_{rotor,\,new} - \zeta_{rotor,\,old}\right|}{\zeta_{rotor,\,old}} < \varepsilon \tag{2}$$

Another value that is calculated is the percentage difference between the thermodynamically calculated rotor exit area and the geometric constraint on the rotor exit area, calculated from Equation (3). This is used to filter out turbine designs where the geometry constrains will not negatively impact the fluid expansion through the stage. By only accepting designs with a low area difference the thermodynamic analysis is supported by the stage geometry.

$$Area\ difference = \frac{A_3 - 2\pi r_{tip,3} b_3}{A_3} \times 100 \tag{3}$$

4. Design Space

The design point of the engine was selected as 5000 rpm at 100% throttle, from which the Ricardo WAVE model was correlated to the best available data to produce design boundary conditions for

the turbocharger; these can be seen in Table 3. The algorithm was initialised with ranges on all design parameters specified in Table 4 and ran the iterative design process with every combination. This resulted in approximately 680,000 design points to be filtered. The D_{max} design ranges were established by the results of a turbocharger scaling process in Ricardo WAVE. The lower end value is the diameter of the scaled radial compressor and the upper limit the scaled radial turbine. It is expected that the larger axial turbines will provide better performance, but at the cost of increased rotational moment of inertia.

Table 3. Design point boundary conditions from Ricardo WAVE.

Engine Speed	**5000 rpm**
Throttle	100%
Exhaust Mass Flow Rate	0.127238 kg/s
Inlet Total Pressure	2.65611 bar
Inlet Total Temperature	1168.55 K
Outlet Static Pressure	1.30352 bar
Turbocharger Speed	158,850 rpm
Produced Power	19.69 kW
Ratio of Specific Heats	1.34
C_p	1168 J/kgK
Specific Speed	0.872794

Table 4. Design parameter ranges.

$\boldsymbol{D_{max}}$ **(mm)**	**49.023–53.43**
HTR	0.45–0.65
ϕ	0.3–0.8
α_3 (°)	0–40
AR_{stator}	0.6–1.4
AR_{rotor}	0.6–1.4
$(\frac{s}{c})_{opt,\ stator}$	0.75–0.95
$(\frac{s}{c})_{opt,\ rotor}$	0.75–0.95
$C_{L,stator}$	0.8–1.2
$C_{L,rotor}$	0.8–1.2

Hub to tip ratio ranges were determined by considering previous experimental designs and considering the required performance along with manufacturing feasibility. The axial turbine turbocharger concept was first demonstrated with HTR = 0.52 Rahnke [8]. Significantly longer blades than this would result in too high stresses, and significantly shorter blades would not provide the desired performance.

The Zweifel coefficient ranges were backed up by literature, with Logan [18] suggesting that 0.8 is the optimum value and Wilson et al. [16] suggesting that modern manufacturing techniques had extended this range from 0.8 up to 1.2.

A tip clearance of 2.5% of blade span was determined. The Ford prototype had a hot running clearance of 3.5% span, however manufacturing methods and tolerances have improved significantly, allowing higer precision devices to be made. Preliminary FEA suggested that spanwise blade deformation would not exceed the 2.5% clearance, so it is physically feasible.

Figure 6 depicts the effect of the design parameter α_3 (absolute gas angle at rotor exit) on the turbine total to static efficiency by plotting individual design points as points coloured by their hub to tip ratio. Higher HTR turbines offer higher efficiency, however with diminishing returns as the lower end of the HTR design range is approached. This effect is due to the definition of tip clearance. As k is a percentage of the blade height, the magnitude of the tip gap is larger for longer blades, which penalises the lower hub to tip ratio designs. There are also clear lines of constant hub to tip ratio that emerge due to the area difference filtering. The design space sweep automatically discards any solutions where

the value of area difference defined in Equation (3) is greater than 1% to ensure the thermodynamic requirements are supported by the stage geometry. These results show that each HTR value will have only have a small number of flow coefficients that it can pair with to produce an area difference <1%.

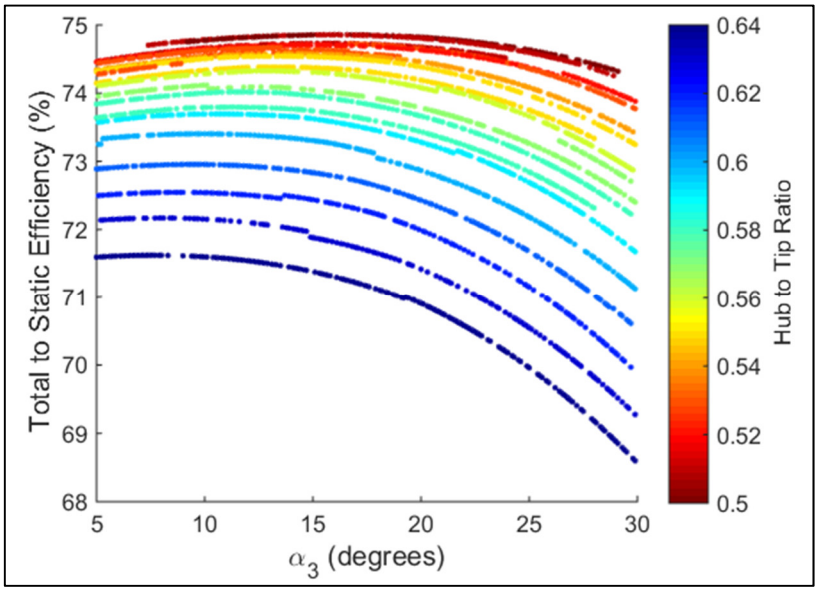

Figure 6. Design space sweep for AR = 0.8, CL = 0.8, (s/c) opt = 0.85, Dmax = 53.43 mm.

Small jumps can be seen along the lines of constant HTR. These are caused by the blade rounding process. Where the system is forcing the number of blades to be at a sub optimal value, for example rounding Z_{rotor} from 14 to 13 to enforce an odd number for vibrational reasons, the efficiency appears to make a small step.

Increasing α_3 reduces the turbine efficiency, however the effect is more prominent on higher hub to tip ratios. This means that choosing a design with longer blades will not penalise high α_3 values as heavily. A concern with low α_3 designs is the reaction at the hub dropping below zero. It was observed that lower hub to tip ratio designs required a higher α_3 before the hub reaction was acceptable. This has a significant effect on the blade geometry at the rotor hub. When α_3 and the reaction are too low, the rotor inlet angle is too high to facilitate a smooth aerofoil profile, with an undesirable bulge appearing at the leading edge.

One of the most important design parameters in the creation of the turbine three-dimensional profile is the aspect ratio, because it is used to determine the blade chord length (Equations (A42) and (A43)). In experimental conditions or CFD analysis increasing the chord length would have a significant effect on the frictional losses from boundary layer viscosity over the blade surface [10]. Using the Ricardo WAVE boundary conditions and providing a set of design parameters while varying the aspect ratios allows the theoretical effect of the blade chord length to be plotted. Figure 7a shows the effect of varying the aspect ratios independently for each blade row as well as in unison. Reducing the chord length of the stator non-linearly increases the total to static efficiency, which suggests that as long the flow is guided and accelerated sufficiently by the stator, additional chord length merely increases frictional losses without providing any benefit. Figure 7a also shows that increasing the aspect ratio of the rotor has a linearly negative impact on the stage efficiency. This suggests that the turbine blades efficiency at expanding the flow is related not just to the flow turning angle and deceleration, but also the distance over which this expansion occurs. The effect of varying the aspect ratios together is dominated by the stator, with a small increase in efficiency for a reduction in chord length on both blade rows.

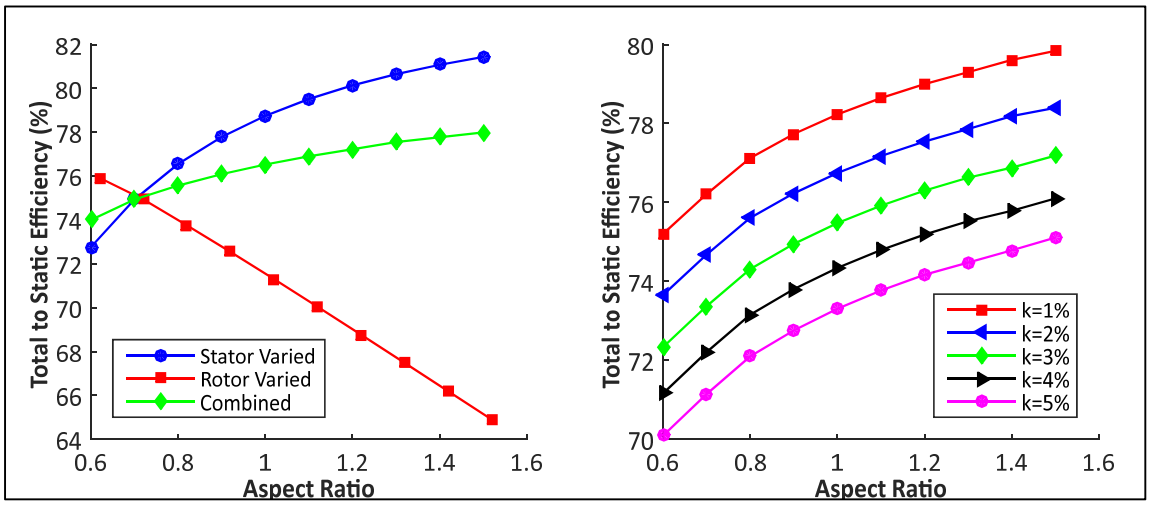

Figure 7. MATLAB predicted effect of aspect ratio for each blade row (**a**) and tip clearance (**b**) on turbine efficiency.

Figure 7b demonstrates that where k is the tip clearance as a percentage of the rotor blade height, increasing k reduces the total to static efficiency by a constant amount. The exception is where the tip clearance is first introduced from 0% to 1%, showing a slightly larger decrease in efficiency than subsequent steps. Increasing rotor chord length does not influence the total tip losses incurred, as each series scales equally with aspect ratio.

The flow coefficient directly determines the axial flow velocity through the turbine stage. Figure 8a suggests that provided the pressure ratio and mass flow rate are maintained, increasing the flow velocity decreases the stage efficiency. This is because the calculation of total to static efficiency includes a term based on the rotor exit velocity. By keeping the stage velocity as low as possible while still producing the required power the system efficiency is increased. The results shown in Figure 6, are mirrored here, where it is again seen that lower hub to tip ratios provide higher efficiencies. Each hub to tip ratio also has a specific blade loading coefficient associated with it, which varies marginally based on the flow coefficient.

Figure 8c,d plot the effect of increasing the design point pressure ratio on a turbine of equal rotational speed or (e) and (f) with an equal mass flow rate. Maintaining a constant design point pressure ratio while increasing the mass flow rate required to achieve it leads to a reduction in total to static efficiency but an increase in power. Increasing the design point pressure ratio will decrease the efficiency of the system but substantially increase the turbine power generation.

It is shown that higher shaft speeds require a higher minimum pressure ratio to support high efficiency operation, however the maximum efficiency that can be reached is also increased. It also suggests that all turbines will experience an efficiency drop-off with a design point pressure ratio that continues to increase. The severity of this drop-off is reduced for higher speed turbines. These results contrast the findings of Alshammari [19] on radial turbines which show an efficiency loss with increased shaft speed. This confirms the earlier discussion around axial turbines increasing in efficiency with specific speed whereas radial turbines suffer performance drop-off [20].

The results of maintaining a design pressure ratio of 2.04, determined by the Ricardo model, while varying the maximum diameter of the turbine can be seen in Figure 8g,h. Higher diameter turbines provide higher efficiency and since this occurs at the same pressure ratio the power is also increased. The shaft speed at which the highest efficiency condition occurs reduces as the size of the turbine increases. This results in smaller turbines providing higher design point efficiencies at very high shaft speeds. For these engine conditions this occurs around 180,000 rpm.

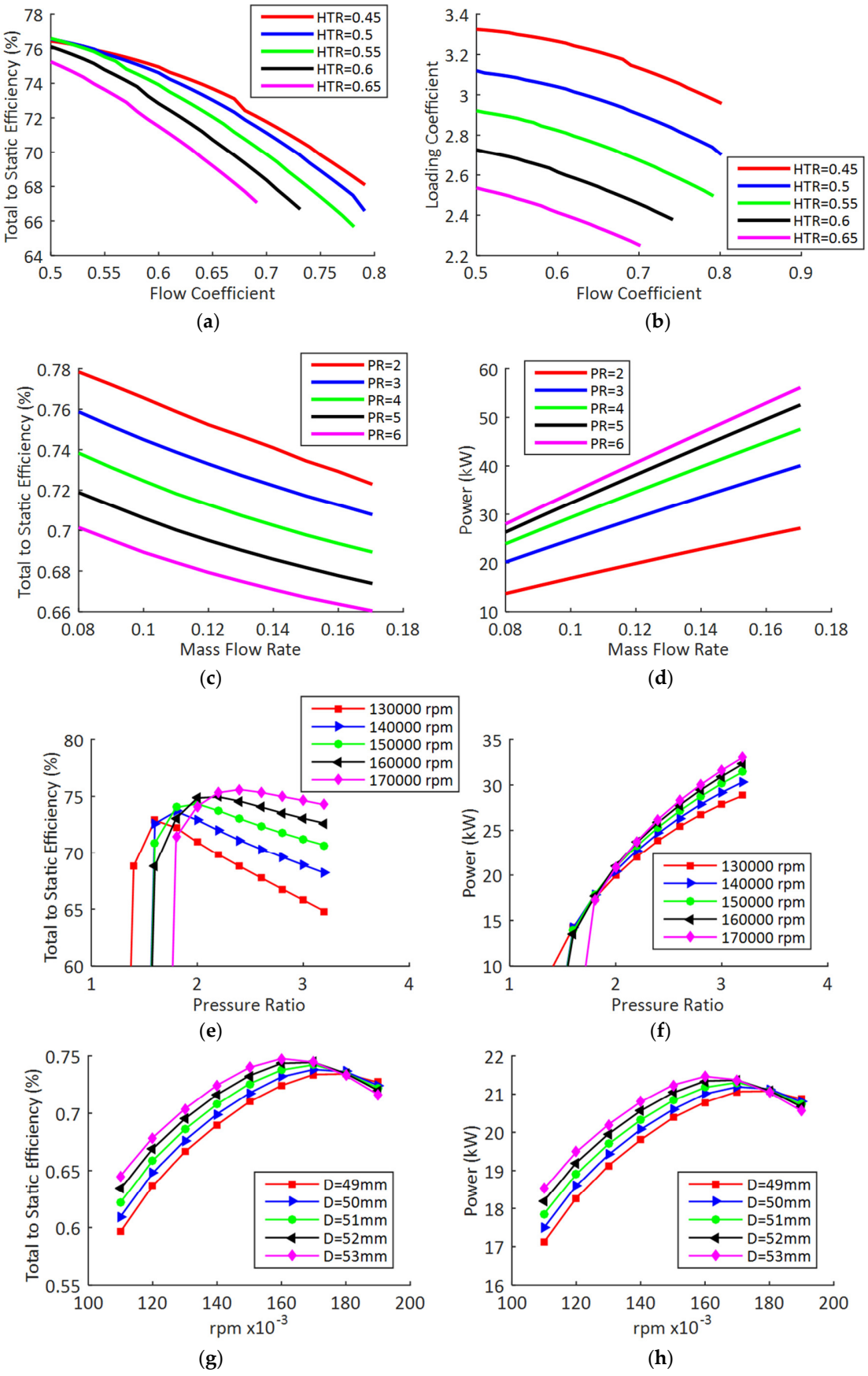

Figure 8. MATLAB predicted effect of flow coefficient (**a**,**b**), mass flow rate (**c**,**d**), pressure ratio (**e**,**f**), and shaft speed (**g**,**h**) on turbine total to static efficiency (**a**,**c**,**e**,**g**) and turbine power (**b**,**d**,**f**,**h**).

5. Preliminary Design

5.1. Preliminary Design Performance Estimation

The design space was sorted based on efficiency and designs with geometric properties not conducive to 'good' blades were filtered out. These included high rotor inlet angles at the hub and unrealistically high stagger angles at the tip. The convergence graphs for the chosen preliminary design point can be seen in Figure 9a,b. The solution converged after 7 iterations and resulted in loss coefficients of $\xi_{stator} = 0.1130$ and $\xi_{rotor} = 0.1807$. This produces a turbine stage with predicted efficiencies of η_{ts} = 74.94 and η_{tt} = 84.20%. The estimated stage reaction at mean span is R = 67.24%. The meanline losses are accurate for the rotor but show a slight overestimate for stator, resulting in slightly lower thermodynamic efficiencies than the Ainley-Mathieson predictions.

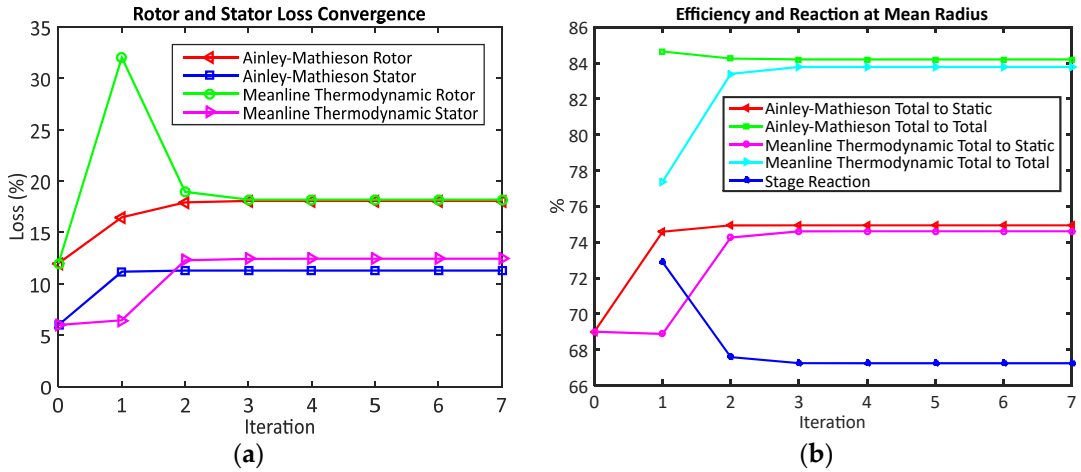

Figure 9. Convergence plots for Ainley-Mathieson and meanline thermodynamic (**a**) losses (**b**) efficiencies.

Trailing edge blockage (TE_b) values were chosen as 0.06 for the stator and 0.08 for the rotor. Logan [18] suggests that values in excess of 0.1 incur significant performance penalties. As this is the preliminary design, the optimum performance is not expected, nor is an acceptable FEA result, but it is important to use realistic values to base the optimisation ranges on. For this reason, a slightly higher value was used for the rotor, as it is under increased loading conditions from both aerodynamic loading and rotational forces (Saravanamuttoo et al. [15]).

Although the blade loss coefficients are directly comparable, they do not themselves identify the enthalpy loss caused by each blade row as the coefficient is multiplied by fluid properties at the relevant station point, as seen in Equation (A71). Figure 9a splits the system enthalpy losses into comparable portions, showing that the rotor is responsible for significantly more enthalpy loss than the stator compared to what the ratio between ξ_{stator} and ξ_{rotor} would suggest (Figure 10). As the total to static efficiency is the performance metric for a single stage turbine, the unrecovered pressure from the exhaust flow is lost. Figure 9a also shows that the magnitude of this enthalpy loss is similar to that of the rotor. It is this loss component that causes the significant efficiency drop between total to total and total to static.

Figure 9b illustrates that stator row losses are dominated by the secondary flow. This explains earlier findings in Figure 7, that showed how influential the stator chord was to system efficiency. The exit loss share is calculated by the magnitude of the trailing edge thickness correction calculated from Figure 5. Had a lower trailing edge blockage value been chosen the effect of this correction could become negative, as the multiplier would drop below unity. Figure 9c depicts the overwhelming importance of minimising tip clearance on the efficiency of the rotor. This high share is due to the increased correlation for Y_k predicted by the Dunham & Came correction for low aspect ratio systems.

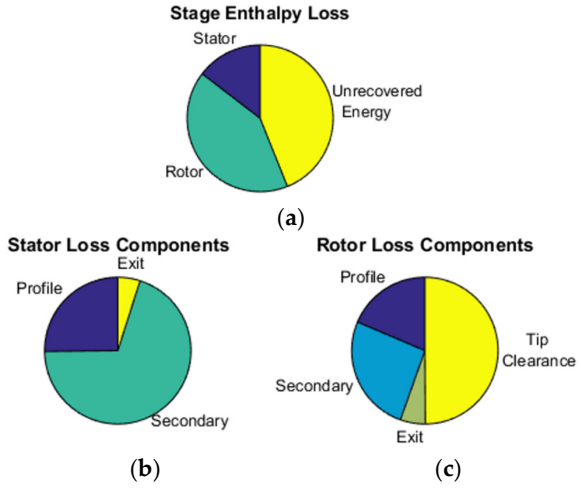

Figure 10. Breakdown of enthalpy losses across (**a**) turbine stage (**b**) stator (**c**) rotor.

To assess the shaft power produced by the turbine the equations in Equations (4) and (5) [17] are used. To double check the MATLAB algorithm an additional method for calculating [6] shaft power was used for cross comparison.

$$\tau = \dot{m} r_{mean} [V_a (\tan(\alpha_{2,mean}) + \tan(\beta_{3,mean})) - \omega r_{mean}] \quad (4)$$

$$P_s = \tau \omega \quad (5)$$

$$P_s = \dot{m} C_p \Delta T_t \quad (6)$$

5.2. Turbine Geometry Generation

To generate the designed blade geometry for validation of the methodology proposed, ANSYS Workbench v18.2, BladeGen application was used. The design parameters outlined in Tables 5 and 6 are written by MATLAB to a generated 'bgi' file, overwriting the existing data. This file is then changed to a 'bgd' type file using a Windows which can be opened in BladeGen. A 3-D view of the blade set it shown in Figure 11.

Table 5. Turbine stage geometry for bgi generate.

Stage Geometry	
b_1 (mm)	7.14
b_2 (mm)	8.53
b_3 (mm)	12.02
b_{stator} (mm)	7.84
b_{rotor} (mm)	9.37
HTR_1	0.71
HTR_2	0.66
HTR_3	0.55
Flare Angle (°)	7.81
Inlet Length (mm)	3.57
Outlet Length (mm)	3
AR_{stator}	0.8
AR_{rotor}	0.82
$C_{L,\ stator}$	0.8
$C_{L,\ rotor}$	0.8
Z_{stator}	20
Z_{rotor}	17
Axial Clearance (mm)	3.22
Rotor Tip Gap (% Span)	2.5

Table 6. Preliminary stator (**a**) and blade profile geometry (**b**) used for bgi generation.

(a) Stator	Hub	Mean	Tip	(b) Rotor	Hub	Mean	Tip
Axial Chord (mm)	6.43	6.43	6.43	Axial Chord (mm)	9.36	6.93	4.63
Stagger Angle (°)	48.96	48.96	48.96	Stagger Angle (°)	41.64	56.45	64.24
Chord (mm)	9.79	9.79	9.79	Chord (mm)	12.52	12.54	10.65
LE Wedge (°)	26	26	26	LE Wedge (°)	24	24	24
TE Wedge (°)	4	4	4	TE Wedge (°)	2	3	2
LE Thickness (mm)	0.35	0.35	0.35	LE Thickness (mm)	0.62	0.45	0.38
TE Thickness (mm)	0.17	0.17	0.17	TE Thickness (mm)	0.22	0.22	0.22

Figure 11. 3-D full view of preliminary design generated.

6. Algorithm Validation

To validate the accuracy of the MATLAB algorithm, CFD simulations were used to determine the thermodynamic properties and turbine performance in comparison to the numerical predictions. The CFD was conducted utilising ANSYS CFX application with turbo mode and the following setup used:

- The fluid is modelled as Air (Ideal Gas)
- K-ω SST turbulence model was chosen.
- Interfaces between stator and rotor, and rotor and outlet are selected as stage (mixing-plane).
- Interfaces between stator blades and interfaces between rotor blades are set as periodic.
- The meshes were setup using ANSYS Turbo Grid consisting of a total of 225,000 nodes.
- Stator blade average Y + 12.2053.
- Rotor blade average Y + 9.8685.

Two CFD cases were run, with Case 1 using total pressure and total temperature at the inlet and a mass flow rate boundary condition at the outlet. This is the most realistic setup for simulating operating conditions, however it did not respond well to choked flow and would often result in numerical instability. The mass flow rate inlet and static pressure outlet boundary conditions were to be used during the design optimisation and turbine map generation. This is labelled as Case 2 in Figure 12.

Using the preliminary design boundary conditions and design parameters the tip gap was varied between k = 0% and k = 5%. The results can be seen in Figure 12a,b. It is worth noting that as the MATLAB algorithm "designs" a turbine based on the input parameters, and k is changing during the sweep, the blade angles would also be changing. For the CFD cases only the tip gap is changed, leaving the rest of the blade geometry identical, meaning that the MATLAB code will certainly be overpredicting the efficiency compared to the CFD in cases other than k = 2.5%.

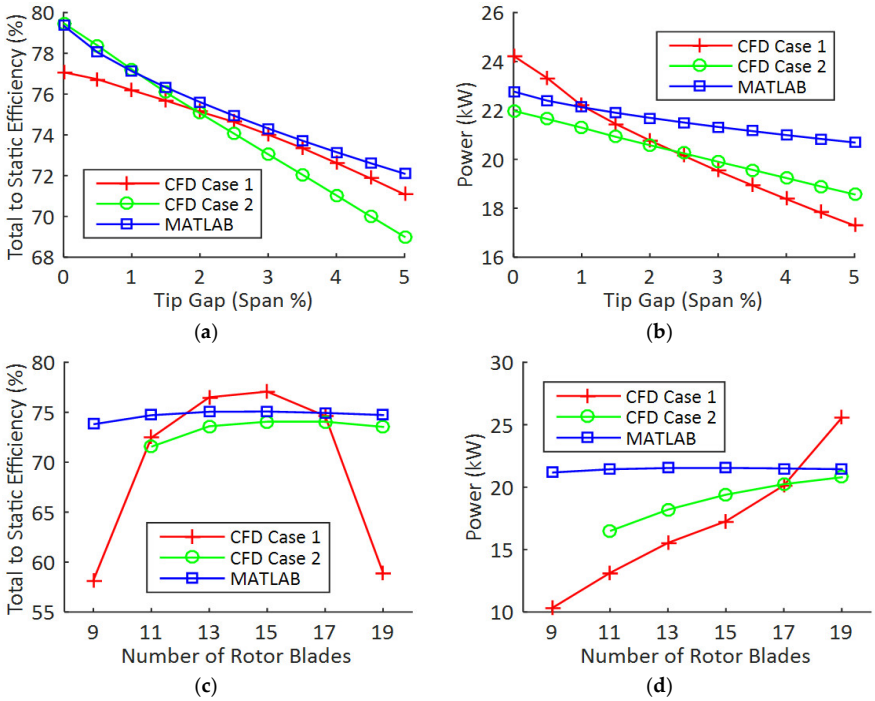

Figure 12. MATLAB algorithm validation for (**a**,**b**) tip gap prediction (**c**,**d**) blade number prediction.

It is illustrated that where k $\leq$ 2%, the total to static efficiency is predicted with less than 1% difference to the CFD result. The gradients begin diverging after this, although this may be due to the overprediction outlined above. When looking at CFD Case 1, modelling free flow conditions, the gradient of the prediction is well matched to the results.

Due to the relationship between the pressure ratio and the turbine power production, CFD Case 1 shows in the blade number sensitivity study that the power generation is heavily based on the throat area. At Z_{rotor} = 9 the power and efficiency of Case 1 results show the fluid is not being accelerated enough to expand the flow and create sufficient torque. By selecting Z_{rotor} = 17 for the design it can be said with confidence that the turbine is producing enough power, rather than being misled by the power output of CFD Case 2. CFD Case 2, by enforcing static pressure at the outlet, inflates the power value compared to what would be experienced in operation. It is also seen that significant over-acceleration of the flow with higher blade numbers causes significant efficiency losses related to the supersonic flow regime. This blade number sensitivity study was conducted where the number of stator blades is always Z_{rotor} + 3.

Table 7 outlines the key stage thermodynamics calculated during the preliminary design algorithm and compares it with the results of CFD Case 2. The CFD results shown are averaged in the radial plane, whereas the MATLAB results are generated from two-dimensional meanline thermodynamic analysis, with the exception of the efficiencies, torque and power.

Table 7. Difference between MATLAB predicted thermodynamics and CFD results.

Parameter	MATLAB	CFD	% Difference
T_1 (K)	1154.82	1152.49	−0.20
T_2 (K)	1099.90	1087.68	−1.12
T_3 (K)	1002.61	984.37	−1.85
T_{t2} (K)	1168.55	1168.62	0.01
T_{t3} (K)	1023.86	1010.02	−1.37
P_1 (bar)	2.54	2.52	−0.44
P_2 (bar)	2.03	2.02	−0.53
P_{t2} (bar)	2.58	2.60	0.61
P_{t3} (bar)	1.42	1.43	0.76

Table 7. *Cont.*

Parameter	MATLAB	CFD	% Difference
M_1	0.26	0.26	0.87
M_2	0.62	0.61	−1.35
M_3	0.36	0.36	−0.35
ρ_1 (kg/m^3)	0.76	0.76	−0.28
ρ_2 (kg/m^3)	0.64	0.65	0.50
ρ_3 (kg/m^3)	0.45	0.46	1.83
η_{ts} (%)	74.94	73.98	−1.29
η_{tt} (%)	84.20	83.46	−0.89
Power (kW)	21.51	20.30	−5.96
Torque (Nm)	1.29	1.22	−5.86

7. Conclusions

Overall it is concluded that the MATLAB algorithm is sufficiently accurate at predicting the stage efficiency and fluid thermodynamics through the stage, demonstrating an accuracy of within 2% of the CFD results for every parameter. However, due to the importance of throat area in the power output, the algorithm overestimates the turbine performance on this metric, displaying an over prediction in the region of 6%. Nevertheless the methodology outlined provides a suitable blade set and a satisfactory starting point for further optimisation.

Author Contributions: G.W., M.B. and G.G. were the students who conducted the project at Brunel University London. A.P. is the turbomachinery group leader in the Centre of Advanced Powertrains and Fuels (CAPF) at Brunel University London, who conceived of the project, the layout of the investigations and checked the computational outcome of the resultant modelling effort and subsequent discussion.

Funding: This research received no external funding.

Conflicts of Interest: The authors declare no conflict of interest.

Appendix A

Meanline Velocity Triangle Analysis Equations [17]

$$r_{tip,3} = \frac{D_{max}}{2} \tag{A1}$$

$$r_{mean} = \frac{r_{tip,3}(1 + HTR)}{2} \tag{A2}$$

$$U_m = \frac{r_{mean}\pi N}{30} \tag{A3}$$

$$\Delta Tt = \eta_{ts} T_{t1} \left[1 - \left(\frac{P_3}{P_{t1}} \right)^{\frac{\gamma-1}{\gamma}} \right] \tag{A4}$$

$$\psi = \frac{2C_p \Delta Tt}{{U_m}^2} \tag{A5}$$

$$\beta_3 = arctan\left(\tan(\alpha_3) + \frac{1}{\phi} \right) \tag{A6}$$

$$R = \phi\beta_3 - \frac{\psi}{4} \tag{A7}$$

$$\beta_2 = arctan\left(\frac{1}{2\phi} \left(\frac{\psi}{2} - 2R \right) \right) \tag{A8}$$

$$\alpha_2 = arctan\left(\tan(\beta_2) + \frac{1}{\phi} \right) \tag{A9}$$

$$V_a = \phi U_m \tag{A10}$$

$$V_2 = \frac{V_a}{\cos(\alpha_2)} \tag{A11}$$

$$V_1 = V_a \tag{A12}$$

$$V_3 = \frac{V_a}{\cos(\alpha_3)} \tag{A13}$$

$$W_2 = \frac{V_a}{\cos(\beta_2)} \tag{A14}$$

$$W_3 = \frac{V_a}{\cos(\beta_3)} \tag{A15}$$

Meanline Fluid Property Analysis Equations [15,17]

$$T_1 = T_{t1} - \frac{{V_a}^2}{2C_p} \tag{A16}$$

$$P_1 = P_{t1}\left(\frac{T_1}{T_{t1}}\right)^{\frac{\gamma}{\gamma-1}} \tag{A17}$$

$$T_2 = T_{t1} - \frac{{V_2}^2}{2C_p} \tag{A18}$$

$$T_{s2} = T_2 - \frac{\xi_{stator}{V_2}^2}{2C_p} \tag{A19}$$

$$P_2 = \frac{P_{t1}}{\left(\frac{T_{t1}}{T_{s2}}\right)^{\frac{\gamma}{\gamma-1}}} \tag{A20}$$

$$P_{t2} = \frac{P_2}{\left(\frac{T_2}{T_{t1}}\right)^{\frac{\gamma}{\gamma-1}}} \tag{A21}$$

$$P_c = P_{t1}\left(\frac{\gamma+1}{2}\right)^{\frac{-\gamma}{\gamma-1}} \tag{A22}$$

$$T_{t3} = T_{t1} - \Delta Tt \tag{A23}$$

$$T_3 = T_{t3} - \frac{{V_3}^2}{2C_p} \tag{A24}$$

$$P_{t3} = \frac{P_3}{\left(\frac{T_3}{T_{t3}}\right)^{\frac{\gamma}{\gamma-1}}} \tag{A25}$$

$$\rho_i = \frac{P_i}{R_{gas}T_i} \tag{A26}$$

$$A_i = \frac{\dot{m}}{\rho_i V_a} \tag{A27}$$

Equations for Calculation of Meanline Thermodynamic Loss Components

Stator Meanline Loss [17]

$$M_2 = \frac{V_2}{\sqrt{\gamma R_{gas}T_2}} \tag{A28}$$

$$Y_{s,meanline} = \frac{P_{t1} - P_{t2}}{P_{t2} - P_2} \tag{A29}$$

$$\xi_{s,meanline} = \frac{Y_{s,meanline}}{1 + (\frac{\gamma-1}{2})M_2^2} \tag{A30}$$

Rotor Meanline Loss [15]

$$T_{ss3} = \frac{T_2}{(\frac{P_2}{P_3})^{\frac{\gamma-1}{\gamma}}} \tag{A31}$$

$$\xi_{r,meanline} = \frac{T_3 - T_{ss3}}{\frac{W_3^2}{2C_p}} \tag{A32}$$

Free Vortex Theory Equations (for stagnation points I = 1,2,3 and span layer j = hub, tip) [15,17]

$$b_i = \frac{A_i}{2\pi r_{mean}} \tag{A33}$$

$$r_{i,tip} = r_{mean} + b_i \tag{A34}$$

$$r_{i,hub} = r_{mean} - b_i \tag{A35}$$

$$\alpha_{i,j} = arctan\left[\left(\frac{r_{mean}}{r_{i,j}}\right) tan(\alpha_{i,mean})\right] \tag{A36}$$

$$\beta_{2,j} = arctan\left[tan(\alpha_{2,j}) - \frac{r_{2,j}}{r_{mean}}\left(\frac{U_m}{V_a}\right)\right] \tag{A37}$$

$$\beta_{3,j} = arctan\left[tan(\alpha_{3,j}) + \frac{r_{3,j}}{r_{mean}}\left(\frac{U_m}{V_a}\right)\right] \tag{A38}$$

$$U_{i,j} = \frac{N\pi r_{i,j}}{30} \tag{A39}$$

Blade Geometry Estimation Equations

Note Equations (A40) to (A47) were obtained from Saravanmutto et al. [15], Equations (A48) to (A53) were obtained from Wilson [16] and Equations (A54) to (A55) were obtained from Logan [18].

$$b_{stator} = \frac{b_1 + b_2}{2} \tag{A40}$$

$$b_{rotor} = \frac{b_2 + b_3}{2} \tag{A41}$$

$$c_{stator} = \frac{b_{stator}}{AR_{stator}} \tag{A42}$$

$$c_{rotor} = \frac{b_{rotor}}{AR_{rotor}} \tag{A43}$$

$$S_{stator,mean} = c_{stator} \times (s/c)_{opt,\ stator} \tag{A44}$$

$$S_{rotor,mean} = c_{rotor} \times (s/c)_{opt,\ rotor} \tag{A45}$$

$$Z_{stator} = \frac{2\pi r_{mean}}{S_{stator,mean}} \tag{A46}$$

$$Z_{rotor} = \frac{2\pi r_{mean}}{S_{rotor,mean}} \tag{A47}$$

$$\sigma_{stator,\ mean} = \left|\left(\frac{2}{C_{L,stator}}\right)\cos^2(\alpha_{2,mean})(tan(\alpha_{1,mean}) - tan(\alpha_{2,mean}))\right| \tag{A48}$$

$$\sigma_{rotor,\ mean} = \left| \left(\frac{2}{C_{L,rotor}} \right) \cos^2(\beta_{3,mean})(tan(\beta_{2,mean}) - tan(\beta_{3,mean})) \right| \tag{A49}$$

$$cx_{stator,mean} = \sigma_{stator,\ mean} \times S_{stator,mean} \tag{A50}$$

$$cx_{rotor,mean} = \sigma_{rotor,\ mean} \times S_{rotor,mean} \tag{A51}$$

$$\lambda_{stator,mean} = arccos\left(\frac{cx_{stator,mean}}{c_{stator,mean}} \right) \tag{A52}$$

$$\lambda_{rotor,mean} = arccos\left(\frac{cx_{rotor,mean}}{c_{rotor,mean}} \right) \tag{A53}$$

$$TE_{thickness_{stator,mean}} = \frac{2TE_{b,s}\pi \cos(\alpha_{2,mean})}{Z_{stator}} \tag{A54}$$

$$TE_{thickness_{rotor,mean}} = \frac{2TE_{b,r}\pi \cos(\beta_{3,mean})}{Z_{rotor}} \tag{A55}$$

Equations for Turbine Stage Performance Prediction

Note Equations (A56) to (A60) were obtained from Ainley and Mathieson [13] and Equations (A61) to (A72) were obtained from Dixon [6] and Saravanmutto et al. [15].

$$Y_{P,rotor} = Y_{P,rotor,\beta_3=0} + \left(\frac{\beta_{2,mean}}{\beta_{3,mean}} \right)^2 (Y_{P,rotor,\beta_2=\beta_3} - Y_{P,rotor,\beta_2=0}) \tag{A56}$$

$$\beta_{m,stator} = arctan\left(\frac{tan(\beta_{3,mean}) - tan(\beta_{2,mean})}{2} \right) \tag{A57}$$

$$\beta_{m,rotor} = arctan\left(\frac{tan(\beta_{3,mean}) - tan(\beta_{2,mean})}{2} \right) \tag{A58}$$

$$C_{L,stator} = 2\left(\frac{S_{stator,mean}}{c_{stator,mean}} \right)(tan(\alpha_{1,mean}) + tan(\alpha_{2,mean}))cos(\beta_{m,stator}) \tag{A59}$$

$$C_{L,rotor} = 2\left(\frac{S_{rotor,mean}}{c_{rotor,mean}} \right)(tan(\beta_{2,mean}) + tan(\beta_{3,mean}))cos(\beta_{m,rotor}) \tag{A60}$$

$$\lambda_{stator} = 0.0334 \frac{c_{stator,mean}}{b_{stator}} \frac{cos(\alpha_{2,mean})}{cos(\alpha_{1,mean})} \tag{A61}$$

$$\lambda_{rotor} = 0.0334 \frac{c_{rotor,mean}}{b_{rotor}} \frac{cos(\beta_{3,mean})}{cos(\beta_{2,mean})} \tag{A62}$$

$$Y_{S,stator} = \lambda_{stator} \left(\frac{C_{L,stator}}{\frac{S_{stator,mean}}{c_{stator,mean}}} \right)^2 \left(\frac{cos^2(\alpha_{2,mean})}{cos^3(\beta_{m,stator})} \right) \tag{A63}$$

$$\begin{aligned} &Y_{S,rotor} + Y_k \\ &= \left[\lambda_{rotor} + 0.47 \frac{c_{rotor,mean}}{b_{rotor}} \left(\frac{b_{rotor}k}{c_{rotor,mean}} \right)^{0.78} \right] \left(\frac{C_{L,rotor}}{S_{rotor,mean}/c_{rotor,mean}} \right)^2 \left(\frac{cos^2(\beta_{3,mean})}{cos^3(\beta_{m,rotor})} \right) \end{aligned} \tag{A64}$$

$$Y_{stator} = Y_{P,stator} + Y_{S,stator} \tag{A65}$$

$$Y_{rotor} = Y_{P,rotor} + Y_{S,rotor} + Y_k \tag{A66}$$

$$Y_{stator,corrected} = Y_{stator} \times TE_{correction,\ stator} \tag{A67}$$

$$Y_{rotor,corrected} = Y_{rotor} \times TE_{correction,\ rotor} \tag{A68}$$

$$\zeta_{stator} = \frac{Y_{stator,corrected}}{\frac{T_{t1}}{T_{s2}}} \tag{A69}$$

$$\xi_{rotor} = \frac{Y_{rotor,corrected}}{\left(\frac{T_3 + \frac{W_3{}^2}{2C_p}}{T_{ss3}}\right)} \tag{A70}$$

$$\eta_{ts} = \left[1 + \frac{\xi_{rotor} W_3{}^2 + \xi_{stator} V_2{}^2 \frac{T_3}{T_2} + V_3{}^2}{2C_p(T_{t1} - T_{t3})}\right]^{-1} \tag{A71}$$

$$\eta_{tt} = \left[1 + \frac{\xi_{rotor} W_3{}^2 + \xi_{stator} V_2{}^2 \frac{T_3}{T_2}}{2C_p(T_{t1} - T_{t3})}\right]^{-1} \tag{A72}$$

Nomenclature

1-3	Station points through the turbine: stator inlet, rotor inlet, rotor exit
A	Area (m^2)
b	Height, passage or blade (m)
c	Blade chord length (m)
c_x	Blade axial chord length (m)
C_L	Zweifel coefficient, Loss model lift coefficient
C_p	Specific heat capacity at constant pressure (J/kgK)
D	Diameter (m)
h	Specific enthalpy (J/kg)
k	Rotor tip clearance (% span)
M	Mach Number
$\dot{m}$	Mass flow rate (kg/s)
N	Turbocharger shaft rotational speed (rpm)
P	Static pressure (Pa)
P_t	Total pressure (Pa)
R	Stage reaction (%)
r	Radius (m)
S	Blade pitch (m)
s	Entropy (kJ/kgK)
T	Static temperature (K)
T_s	Isentropic static temperature (K)
T_t	Total temperature (K)
TE_b	Trailing edge blockage
U	Rotor blade linear velocity (m/s)
V	Absolute flow velocity (m/s)
W	Relative flow velocity (m/s)
Y	Pressure loss coefficient
Z	Number of blades
α	Absolute flow angle (°)
β	Relative flow angle (°)
γ	Ratio of specific heats
ε	Convergence criteria
η	Isentropic expansion efficiency (%)
λ	Blade stagger angle (°), Secondary loss coefficient
ξ	Enthalpy loss coefficient
ρ	Density (kg/m^3)
σ	Axial solidity
ϕ	Flow coefficient
ψ	Blade loading coefficient

Abbreviations

bgd	BladeGen geometry file
bgi	BladeGen batch input file
HTR	Hub to Tip Ratio
LE	Leading Edge
TE	Trailing Edge
CFD	Computational Fluid Dynamics
FEA	Finite Element Analysis

References

1. Fraser, N.; Blaxill, H.; Lumsden, G.; Basset, M. Challenges for Increased Efficiency through Gasoline Engine Downsizing. *SAE Int. J. Eng.* **2009**, *2*, 991–1008. [CrossRef]
2. Department for Business, Energy & Industrial Strategy. Statistical Data Set-Weekly Road Fuel. 2018. Available online: https://www.gov.uk/government/statistical-data-sets/oil-and-petroleum-products-weekly-statistics (accessed on 16 April 2018).
3. Rate Inflation. United Kingdom Consumer Price Index (CPI) History—2008 to 2018. 2018. Available online: https://www.rateinflation.com/consumer-price-index/uk-historical-cpi (accessed on 16 April 2018).
4. Simmons, A.; Giakoumis, E. *Turbochargers and Turbochargind: Advancements, Applications and Research*; Nova Science Publisher: New York, NY, USA, 2017.
5. Cammisa, J. Why Ferrari Engineers Don't Like Turbos. 8 January 2015. Available online: https://www.roadandtrack.com/car-culture/news/a24691/ferrari-engineers-dont-liketurbocharging/ (accessed on 16 April 2018).
6. Dixon, S.; Hall, C. *Fluid Mechanics, Thermodynamics of Turbomachinery*; Butterworth: Oxford, UK, 2014.
7. Pesiridis, A.; Saccomanno, A.; Tuccillo, R.; Capobianco, A. Conceptual Design of a Variable Geometry, Axial Flow Turbocharger Turbine. 2017. Available online: https://bura.brunel.ac.uk/handle/2438/15484 (accessed on 16 April 2018).
8. Balje, O. *Turbomachines—A Guide to Design, Selection, and Theory*; Wiley: New York, NY, USA, 1981.
9. Rahnke, C. Axial Flow Automotive Turbocharger. In Proceedings of the ASME Gas Turbine Conference and Exhibit, Houston, TX, USA, 18–21 March 1985.
10. Bauer, H.; Bali, C.; Donkin, G.; Davies, P. *The Next Generation of Gasoline Turbo Technology*; Honeywell Transportation Systems: Rolle, Switzerland, 2012.
11. Wei, N. *Significance of Loss Models in Aerothermodynamic Simulation for Axial Turbines*; Royal Institute of Technology (KTH): Stockholm, Sweden, 2000.
12. Soderberg, C. *Unpublished Notes, Gas Turbine Laboratory*; Massachusetts Institute of Technology: Cambridge, MA, USA, 1949.
13. Craig, H.; Cox, H. Performance Estimation of Axial Flow Turbines. *Proc. Inst. Mech.Eng.* **1970**, *185*, 407–424. [CrossRef]
14. Ainley, D.; Mathieson, G. *A Method of Performance Estimation for Axial-Flow Turbines*; Aeronautical Research Council London: London, UK, 1951.
15. Yaras, M.; Sjolander, S. Prediction of Tip-Leakage Losses in Axial Turbines. *J. Turbomach.* **1992**, *114*, 204–210. [CrossRef]
16. Saravanamuttoo, H.; Rogers, G.; Cohen, H. *Gas Turbine Theory*, 5th ed.; Pearson Education: Harlow, UK, 2001.
17. Wilson, D.; Korakianitis, T. *The Design of High Efficiency Turbomachinery and Gas Turbines*, 2nd ed.; Prentice-Hall: Upper Saddle River, NJ, USA, 1998.
18. Peng, W. *Fundamentals of Turbomachinery*; John Wiley & Sons: Hoboken, NJ, USA, 2008.
19. Logan, E. *Handbook of Turbomachinery*; Marcel Dekker: New York, NY, USA, 1995.
20. Alshammari, F. *Radial Turbine Expander Design, Modelling and Testing for Automotive Organic Rankine Cycle Waste Heat Recovery*; Brunel University: London, UK, 2018.